ISBN: 978-3-95450-233-2 ISSN: 2673-5504 doi:10.18429/JACoW-SRF2021-SUPFDV002

AB INITIO THEORY OF THE IMPACT OF GRAIN BOUNDARIES ON THE SUPERCONDUCTING PROPERTIES OF Nb_3Sn *

M. M. Kelley†, T. A. Arias and N. Sitaraman, Cornell University, Ithaca, NY 14853, USA

Abstract

Grain boundaries significantly affect the superconducting properties of Nb_3Sn, and for SRF applications, grain boundaries can provide weak points for vortex entry and ultimately limit the efficiency of Nb_3Sn SRF cavities. Here we use density functional theory (DFT) to investigate the physics of different grain boundary types in Nb_3Sn and distinguish the properties of clean grain boundaries from grain boundaries containing tin antisite defects. Clean grain boundaries reduce the Fermi-level density of states by over a factor of two, and the bulk electronic structure is recovered ∼1 nm from the boundary plane. We use atomic concentration measurements of an SRF cavity to determine the effects of tin-segregation on grain boundaries and find that tin-rich boundaries widen the reduction in the Fermi-level density of states out to ∼1.5 nm from the boundary plane, producing a full width of ∼3 nm. Finally, we introduce a model for a local superconducting transition temperature T_c as a function of distance from the boundary plane, and provide a new estimate for flux-pinning forces based on our DFT calculations.

INTRODUCTION

Nb_3Sn is a type-II superconductor with a critical temperature of 18 K and is a promising material for next-generation SRF cavities [1, 2]. The ∼3 nm coherence length of Nb_3Sn is considerably shorter than the ∼50 nm coherence length of elemental superconductor Nb, making the material much more sensitive to defects such as grain boundaries [3–5].

For SRF applications, grain boundaries can provide nucleation sites for flux to penetrate and lead to significant dissipation. [6–9]. In particular, strong Q-slopes have been observed in SRF cavities with prominent tin segregation at grain boundaries [10]. Furthermore, studies of superconducting wires show that strong gradients of tin composition at grain boundaries can reduce the critical current density, the flux pinning force, and flux pinning scaling field [11–13].

Despite many experimental and numerical studies pointing out the importance grain boundaries in Nb_3Sn, only recently has a study thoroughly investigated the physics of grain boundaries in Nb_3Sn using first principles calculations [14].

Here we study the influence of grain boundaries on the properties of Nb_3Sn from first principles using density functional theory (DFT). We calculate the impact of grain boundaries on the material's electronic structure, and go on to calculate the effect of grain boundaries containing atomic concentrations corresponding to measurements of Nb_3Sn SRF cavities exhibiting strong Q-slopes [10]. Finally, we provide estimates for local superconducting properties including a model for a local T_c and flux-pinning force.

METHODS

We perform DFT calculations with open-source plane wave software JDFTx using the pseudopotential framework [15]. The electronic states are calculated for the valence and semi-core electrons of niobium ($4p^6 5s^2 4d^3$) and tin ($4d^{10} 5s^2 5p^2$), and the atomic cores are approximated using ultrasoft pseudopotentials [16]. We use the Perdew-Burke-Ernzerhof (PBE) approximation to the exchange-correlation functional and employ a 12 Hartree planewave cutoff energy [17]. We calculated zero-temperature effects using the cold-smearing method developed by Marzari with a smearing width of 5 mH [18]. For cubic A15 Nb_3Sn, we sample 6^3 k-points in the Brillouin zone and its density of states is calculated with a dense Monte Carlo sampling in a maximally localized Wannier function basis [19]. The k-point meshes for the grain-boundary cells contain comparable sampling densities as the unit cell calculation, and their densities of states are calculated with tetrahedral interpolation. The lattice parameter for cubic A15 Nb_3Sn is calculated to be 5.271 Å, agreeing well with its measured value of 5.289 Å [20, 21]. We allow the lattices of the grain-boundary cells to relax along the boundary plane normal but find that the lattice relaxations do not produce any significant changes, and consequently, we choose to report results calculated at the bulk lattice constant. All the boundary cells reported in this paper contain fully relaxed internal atomic coordinates.

SUPERCONDUCTIVITY IN THE A15 STRUCTURE

Nb_3Sn is part of the A15 class of conventional superconductors which held the record for highest T_c from 1954–1986 [22, 23]. The A15 structure is shown in Fig. 1(a), with tin atoms in red forming a BCC lattice and niobium atoms in blue forming long chains that span the faces of the cubic unit cell.

A common feature of the A15 superconductors is their high Fermi-level density of states. The total density of states for Nb_3Sn is plotted in 1(b). The value at the Fermi-level is indeed high and also sharply drops by nearly a factor of 5 within ∼0.2 eV. The shape of the density of states in Nb_3Sn is attributed to the d-orbitals of the chains of Nb atoms in the A15 phase. Figure 1(c) demonstrates this relationship by displaying the partial projected density of states along d-orbitals of the Nb atoms.

* This work was supported by the U.S. National Science Foundation under Award PHY-1549132, the Center for Bright Beams.
† mmk255@cornell.edu

ISBN: 978-3-95450-233-2 ISSN: 2673-5504 doi:10.18429/JACoW-SRF2021-SUPFDV002

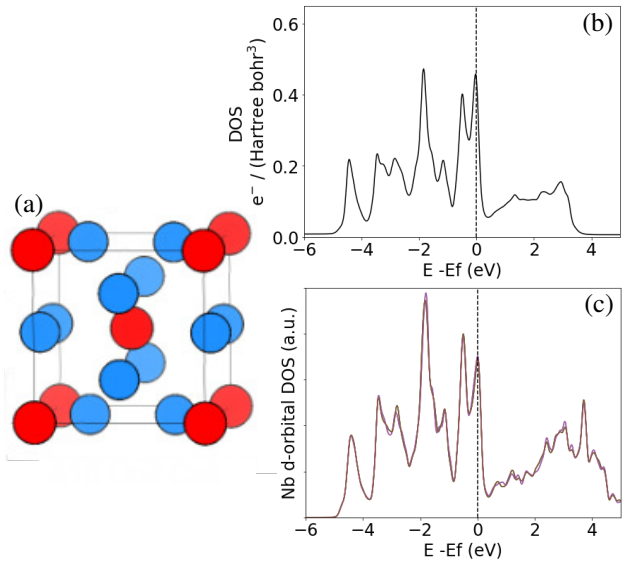

Figure 1: (a) The A15 unit cell for Nb_3Sn with tin in red and niobium in blue. (b) The total density of states for Nb_3Sn and (c) the partial projected density of states onto the d-orbitals of the niobium atoms.

The high Fermi-level density of states of the A15 superconductors contributes to their high critical temperatures. One can see this from the BCS equation,

$$k_B T_c = 1.14 E_D e^{-1/N(0)V} \quad (1)$$

where E_D denotes the Debye energy, $N(0)$ denotes the Fermi-level density of states, and V is the electron-phonon coupling potential. For strongly-coupled superconductors such as Nb_3Sn, the BCS equation is replaced by the McMillan equation, but regardless, the superconducting critical temperature has an exponential dependence on the Fermi-level density of states.

The properties of Nb_3Sn, including its density of states, are known to be sensitive to disorder and stoichiometric variations that interrupt the long conducting chains of Nb atoms [5, 20, 24, 25]. While the effect of point defects has been well studied in Nb_3Sn, here we show how grain boundaries affect the material.

Table 1: Summary of boundary cells

Boundary	Number of atoms	Grain separation	θ	γ [mJ m^{-2}]
(112)-RT	192	2.59 nm	70.5°	840
(110)-RT	128	2.99 nm	90°	1455

Grain Boundary Structures

A summary of the grain boundary structures presented in this paper are shown in Table 1. Results for more grain boundary systems and a description of the interfacial energy, γ, can be found in Ref. [14].

Figures 2(a) and (b) show the d-orbital projected density of states for Nb atoms in the grain boundary core and the bulk region of the (112)-RT grain boundary system, respectively. The latter displays that the bulk electronic structure is restored between the grain boundaries, indicating that the system is converged with respect to the separation between grains. The Fermi-level density of states for the Nb atoms within the grain boundary core reduces by over a factor of two. To emphasize the severity of this reduction, a global reduction of this amount would drop the material's critical temperature to below 10 K.

LOCAL IMPACT ON ELECTRONIC STRUCTURE

Clean Grain Boundaries

The (112)-RT grain boundary cell contains Nb_3Sn's preferred 3:1 stoichiometry ratio, and this property defines a clean grain boundary. The spatial extent of reduction in the Fermi-level density of states by the (112)-RT boundary is shown in Fig. 2(c). The Fermi-level density of states is reduced by over a factor of two at the grain boundary core and this reduction smoothly decays until the bulk electronic structure is restored $\sim$1 nm from the boundary plane.

Tin-rich Grain Boundaries

To probe the effects of grain boundary composition on the local electronic structure, we calculate the impact of a grain boundary containing tin-concentrations that match the SRF cavity atomic measurements reported in Ref. 10. They identify a $\sim$3 nm wide boundary with a maximum tin concentration at 35% and a Gibbsian interfacial excess of 10–20 tin atoms/nm^2. To ensure we do not overestimate the effects of tin-segregation to grain boundaries, we add an excess of only 10 tin atoms/nm^2 extending $<$3 nm in our (110)-RT grain boundary cell.

The local Fermi-level density of states profiles from the clean (110)-RT and the same structure with excess tin atoms are displayed in Fig. 3. The profile of the clean (110)-RT extends $\sim$1 nm out from the boundary plane, just as we found for the (112)-RT in Fig. 2(c). However, the depleted region in the tin-rich grain boundary widens to slightly over $\sim$1.5 nm, yielding a full width of $\sim$3 nm.

ESTIMATES FOR LOCAL SUPERCONDUCTING PROPERTIES

Local T_c

To understand the impact of grain boundary composition on the local superconducting properties, we focus on changes in the Fermi-level density of states and neglect changes in the phonon spectrum. This approximation is justified by a first principles study on the impact on strain in Nb_3Sn, showing that $\sim$80% of the degradation of the superconducting properties from strain comes from the reduction in the Fermi-level density of states [27], and another first principles study on

ISBN: 978-3-95450-233-2 ISSN: 2673-5504 doi:10.18429/JACoW-SRF2021-SUPFDV002

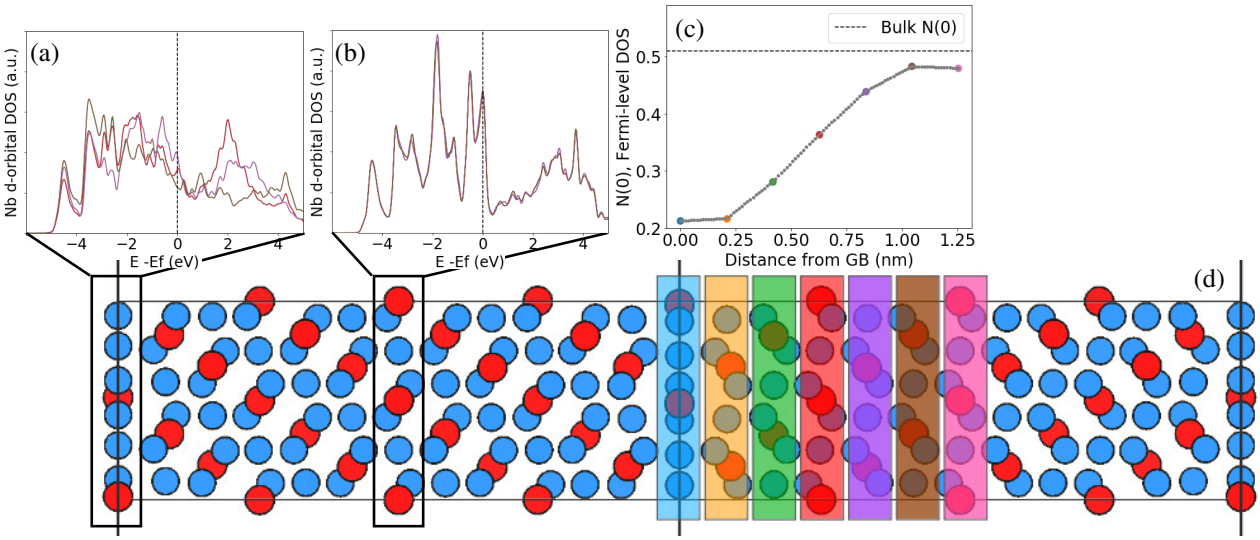

Figure 2: The partial projected density of states onto the d-orbitals of (a) niobium atoms within the grain boundary core and (b) niobium atoms in the bulk region of the grain boundary cell, demonstrating convergence of the bulk density of states. Local density of states profile showing (c) the total density of states at the Fermi-level a function of distance from the boundary plane within (d) the (112)-RT grain boundary unit cell [26].

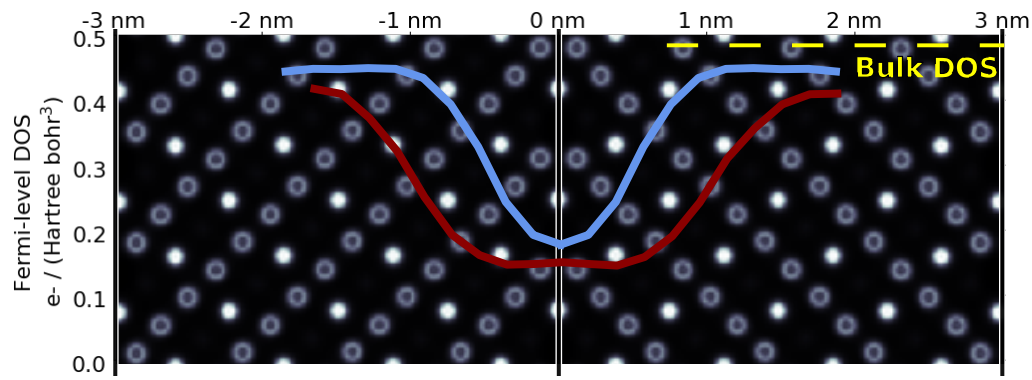

Figure 3: The local Fermi-level density of states profiles from a clean boundary (light blue) and a tin-rich boundary (dark red) overlaid on top of a slice of the electronic density in the clean (110)-RT boundary cell (grayscale colormap). The tin-rich boundary is calculated by taking the same structure as the clean boundary and imposing tin antisite defects to yield tin concentrations analogous to the atomic measurements on the SRF cavity reported in Ref. [10].

antisite defects in Nb_3Sn finding T_c to be strongly correlated with the Fermi-level density of states [5].

To provide an estimate for a local superconducting critical temperature, the Fermi-level density of states should first be averaged over the appropriate length scale, specifically the coherence length Nb_3Sn. The top panel in Fig. 4 shows estimates for the local transition temperature, obtained by integrating the density of states profiles in Fig. 3 over spheres of radii 3 nm and 5 nm, demonstrating the sensitivity of the estimate with respect to averaging.

The reduction in T_c is wider and much deeper for the tin-rich boundary than for the clean boundary as a result of the much wider depression in the local Fermi-level density of states. The boundary containing excess tin widens the depression in the density of states, to the detriment of the local superconducting properties.

Local Flux Pinning Force

Our DFT calculations can also be used to generate estimates for local flux pinning forces at grain boundaries. An expression for the flux pinning force per unit length can be derived from the condensation energy per unit length of a vortex line, ϵ_1, found in Tinkham's *Introduction to Superconductivity*:

$$f_{\text{pin}} = \frac{\partial \epsilon_1}{\partial x} = \frac{H_{c2}}{2\kappa^2}\xi^2 \log(\kappa)\frac{\partial H_{c2}}{\partial x} \propto \max\left(\frac{\partial T_c}{\partial x}\right). \quad (2)$$

We determine the local flux pinning force per unit length from the maximum of the gradient in T_c, the force required to completely unpin the vortex line from the boundary.

ISBN: 978-3-95450-233-2 ISSN: 2673-5504 doi:10.18429/JACoW-SRF2021-SUPFDV002

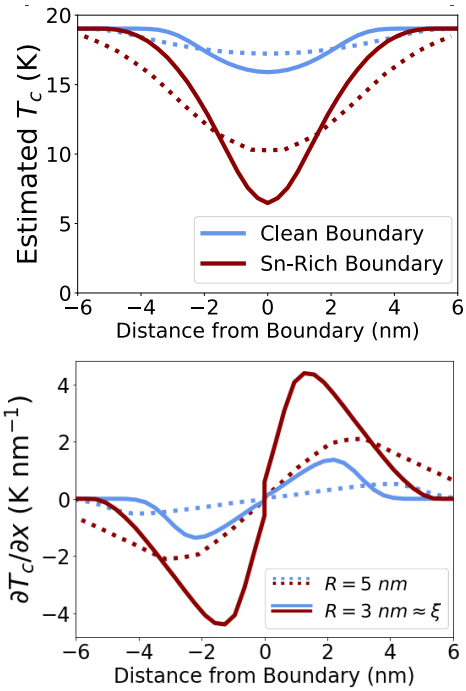

Figure 4: Models of local superconducting properties estimating (top) T_c a function of distance from the grain boundary plane, generated by averaging the profiles in Fig. 3 over spheres with radii comparable to the coherence length in Nb_3Sn and (bottom) the corresponding local gradients of the T_c profiles in the top panel used to estimate flux pinning forces.

The bottom panel in Fig. 4 shows the local gradient in T_c corresponding to the local T_c profiles in the top panel of the figure.

From the pinning force, we can predict the value of the accelerating field at which a vortex line becomes unpinned and penetrates the bulk of the material by relating the flux pinning force to the opposing force created by the field within the SRF cavity. This opposing force is the Lorentz force per unit length,

$$f_L = \frac{\phi_0 H_{RF}}{\lambda}, \quad (3)$$

where ϕ_0 is the flux quantum and λ is the penetration depth.

By equating the Lorentz force with the flux pinning force, a maximum gradient T_c of 4 K/nm would imply that the Lorentz force overcomes the pinning force at ∼5 MV/m for a TESLA cavity. This result correlates well with the findings of Ref. 10, reporting strong Q-slopes from Nb_3Sn SRF cavities containing tin-rich grain boundaries, where the onset of the Q-slope can be seen ∼5 MV/m.

Despite this promising agreement, we must point out shortcomings of this current model. By taking the gradient after the spherical-averaging procedure discussed in the previous section, this model currently predicts that the pinning in clean grain boundaries is weaker than in tin-rich boundaries, which we believe is incorrect. This prediction is an artifact of the current averaging procedure, but we can also directly use the local Fermi-level density of states, a well-defined physical quantity, to provide an upper-bound to this pinning force estimates. Assuming that the local superconducting properties are determined directly from the local Fermi-level density of states, we find a maximum $\partial T_c/\partial x$ of 15 K/nm for both the clean and tin-rich boundaries, corresponding to an unpinning field of ∼17–22 MV/m for a TESLA cavity. However, the positions of the maximums in $\partial T_c/\partial x$ appear at ∼0.6 nm for the clean grain boundary and at ∼1 nm for the tin-rich. Furthermore, $\partial T_c/\partial x$ decays to zero ∼1.5 nm away from the clean grain boundary but is still >10 K/nm over 2 nm away from the tin-rich grain boundary. We are continuing to develop this DFT flux pinning force model and will be supplementing with Ginzburg-Landau simulations to account for size-effects of the vortex line.

CONCLUSIONS

Using DFT, we study grain boundaries in Nb_3Sn and find that they have a strong impact on the material's superconducting properties [14]. Grain boundaries significantly degrade the Fermi-level density of states, which is expected from the disrupted d-orbitals from the chains of niobium atoms in the A15 phase. The Fermi-level density of states drops by over a factor of two at the grain boundary core, and if this effect were global, T_c would drastically drop to under 10 K. The reduction in the density of states from grain boundaries is found to extend out to ∼1 nm from a clean boundary and out to ∼1.5 nm from a boundary containing tin-concentrations analogous to the atomic measurements of an SRF cavity reported in Ref. 10.

We introduce a model for a local superconducting transition temperature and find the reduction in T_c to be wider and much deeper for the tin-rich boundary than for the clean boundary as a result of the much wider depression in the local Fermi-level density of states. The local T_c around a clean grain boundary is barely degraded because the depression in the density of states has a diameter of ∼2 nm while a Cooper pair has a radius of 3 nm. However, a grain boundary filled with tin-defects widens the depression in the density of states, to the detriment of the local superconducting properties. This result correlates well with the findings of Ref. 10, reporting degraded quality factors from Nb_3Sn SRF cavities containing tin-rich grain boundaries and high quality factors from cavities containing clean grain boundaries.

Our DFT calculations can also be used to provide estimates for flux pinning forces, and we present preliminary results suggesting that vortices may become unpinned at fields as low as ∼5 MV/m, and provide initial estimates for an upper bound at fields around ∼17–22 MV/m. However, this DFT flux pinning model requires further development taking into account size effects of vortex lines in order to provide more accurate, quantitative estimates.

Grain boundaries with low T_c are a promising mechanism that lowers the first vortex entry field in Nb_3Sn SRF cavities, and Ginzburg-Landau simulations can build off of these local T_c estimates to further our understanding of flux pen-

ISBN: 978-3-95450-233-2 ISSN: 2673-5504 doi:10.18429/JACoW-SRF2021-SUPFDV002

etration and pinning at grain boundaries, and in particular, dissipation in Nb_3Sn SRF cavities [7, 9, 12].

ACKNOWLEDGEMENTS

We would like to thank Jim Sethna, David Muller, Matthias Liepe, and Ryan Porter of Cornell University, Sam Posen of Fermilab, Jaeyel Lee and David Seidman of Northwestern University, and Ravishankar Sundararaman of Rensselaer Polytechnic Institute.

REFERENCES

[1] S. Posen, M. Liepe, and D. L. Hall, "Proof-of-principle demonstration of Nb_3Sn superconducting radiofrequency cavities for high Q_0 applications," *Appl. Phys. Lett.*, vol. 106, no. 8, pp. 0–4, 2015.

[2] R. D. Porter, T. Arias, P. Cueva, D. L. Hall, M. Liepe, J. T. Maniscalco, D. A. Muller, and N. Sitaraman, "Next generation Nb_3Sn SRF cavities for linear accelerators," in *Proceedings of LINAC2018*, pp. 462–465, 2018.

[3] M. Suenaga and W. Jansen, "Chemical compositions at and near the grain boundaries in bronze-processed superconducting Nb_3Sn," *Appl. Phys. Lett.*, vol. 43, no. 8, pp. 791–793, 1983.

[4] M. J. Sandim, D. Tytko, A. Kostka, P. Choi, S. Awaji, K. Watanabe, and D. Raabe, "Grain boundary segregation in a bronze-route Nb_3Sn superconducting wire studied by atom probe tomography," *Supercond. Sci. Technol.*, vol. 26, no. 5, p. 055008, 2013.

[5] N. S. Sitaraman, J. Carlson, A. R. Pack, R. D. Porter, M. U. Liepe, M. K. Transtrum, and T. A. Arias, "Ab Initio Study of Antisite Defects in Nb_3Sn: Phase Diagram and Impact on Superconductivity arXiv:1912.07576," 2019.

[6] S. Posen and D. L. Hall, "Nb_3Sn superconducting radiofrequency cavities: Fabrication, results, properties, and prospects," *Supercond. Sci. Technol.*, vol. 30, no. 3, p. 033004, 2017.

[7] M. K. Transtrum, G. Catelani, and J. P. Sethna, "Superheating field of superconductors within Ginzburg-Landau theory," *Phys. Rev. B*, vol. 83, no. 9, pp. 1–8, 2011.

[8] D. B. Liarte, S. Posen, M. K. Transtrum, G. Catelani, M. Liepe, and J. P. Sethna, "Theoretical estimates of maximum fields in superconducting resonant radio frequency cavities: Stability theory, disorder, and laminates," *Supercond. Sci. Technol.*, vol. 30, no. 3, pp. 0–22, 2017.

[9] J. Carlson, A. Pack, M. K. Transtrum, J. Lee, D. N. Seidman, D. B. Liarte, N. Sitaraman, A. Senanian, J. P. Sethna, T. Arias, and S. Posen, "Analysis of magnetic vortex dissipation in Sn-segregated boundaries in Nb_3Sn SRF cavities arXiv:2003.03362," 2020.

[10] J. Lee, Z. Mao, K. He, Z. H. Sung, T. Spina, S. I. Baik, D. L. Hall, M. Liepe, D. N. Seidman, and S. Posen, "Grain-boundary structure and segregation in Nb_3Sn coatings on Nb for high-performance superconducting radiofrequency cavity applications," *Acta Mater.*, vol. 188, pp. 155–165, 2020.

[11] L. D. Cooley, C. M. Fischer, P. J. Lee, and D. C. Larbalestier, "Simulations of the effects of tin composition gradients on the superconducting properties of Nb_3Sn conductors," *J. Appl. Phys.*, vol. 96, no. 4, pp. 2122–2130, 2004.

[12] Y. Li and Y. Gao, "GLAG theory for superconducting property variations with A15 composition in Nb_3Sn wires," *Sci. Rep.*, vol. 7, no. 1, pp. 1–13, 2017.

[13] T. Baumgartner, S. Pfeiffer, J. Bernardi, A. Ballarino, and M. Eisterer, "Effects of inhomogeneities on pinning force scaling in Nb_3Sn wires," *Supercond. Sci. Technol.*, vol. 31, no. 8, p. 084002, 2018.

[14] M. M. Kelley, N. S. Sitaraman, and T. A. Arias, "Ab initio theory of the impact of grain boundaries and substitutional defects on superconducting nb3sn," *Superconductor Science and Technology*, vol. 34, p. 015015, dec 2020.

[15] R. Sundararaman, K. Letchworth-Weaver, K. A. Schwarz, D. Gunceler, Y. Ozhabes, and T. A. Arias, "JDFTx: Software for joint density-functional theory," *SoftwareX*, vol. 6, pp. 278–284, 2017.

[16] K. F. Garrity, J. W. Bennett, K. M. Rabe, and D. Vanderbilt, "Pseudopotentials for high-throughput DFT calculations," *Comput. Mater. Sci.*, vol. 81, pp. 446–452, 2014.

[17] J. P. Perdew, K. Burke, and M. Ernzerhof, "Generalized gradient approximation made simple," *Phys. Rev. Lett.*, vol. 77, no. 18, pp. 3865–3868, 1996.

[18] N. Marzari, D. Vanderbilt, A. De Vita, and M. C. Payne, "Thermal contraction and disordering of the Al(110) surface," *Phys. Rev. Lett.*, vol. 82, no. 16, pp. 3296–3299, 1999.

[19] N. Marzari and D. Vanderbilt, "Maximally localized generalized Wannier functions for composite energy bands," *Phys. Rev. B*, vol. 56, no. 20, pp. 12847–12865, 1997.

[20] A. Godeke, "A review of the properties of Nb_3Sn and their variation with A15 composition, morphology and strain state," *Supercond. Sci. Technol.*, vol. 19, no. 8, p. R68, 2006.

[21] H. Devantay, J. L. Jorda, M. Decroux, J. Muller, and R. Flükiger, "The physical and structural properties of superconducting A15-type Nb-Sn alloys," *J. Mater. Sci.*, vol. 16, no. 8, pp. 2145–2153, 1981.

[22] D. Dew-Hughes, "Superconducting A-15 compounds: A review," *Cryogenics*, vol. 15, no. 8, pp. 435–454, 1975.

[23] G. R. Stewart, "Superconductivity in the A15 structure," *Phys. C Supercond. its Appl.*, vol. 514, pp. 28–35, 2015.

[24] M. G. T. Mentink, M. M. J. Dhalle, D. R. Dietderich, A. Godeke, F. Hellman, and H. H. J. ten Kate, "The effects of disorder on the normal state and superconducting properties of Nb_3Sn," *Supercond. Sci. Technol.*, vol. 30, no. 2, p. 25006, 2017.

[25] R. Flükiger, D. Uglietti, C. Senatore, and F. Buta, "Microstructure, composition and critical current density of superconducting Nb_3Sn wires," *Cryogenics*, vol. 48, no. 7-8, pp. 293–307, 2008.

[26] K. Momma and F. Izumi, "VESTA3 for three-dimensional visualization of crystal, volumetric and morphology data," *J. Appl. Crystallogr.*, vol. 44, no. 6, pp. 1272–1276, 2011.

[27] A. Godeke, F. Hellman, H. H. Kate, and M. G. Mentink, "Fundamental origin of the large impact of strain on superconducting Nb_3Sn," *Supercond. Sci. Technol.*, vol. 31, no. 10, p. 105011, 2018.